

V-ATPase Disassembly at the Yeast Lysosome-Like Vacuole Is a Phenotypic Driver of Lysosome Dysfunction in Replicative Aging

Fiza Hashmi and Patricia M. Kane

Department of Biochemistry and Molecular Biology
SUNY Upstate Medical University, Syracuse, NY USA

Address correspondence to: Patricia M. Kane
kanepm@upstate.edu

Running title: V-ATPase disassembly in replicative aging

1 Declines in lysosomal acidification and function with aging are observed in organisms
2 ranging from yeast to humans. V-ATPases play a central role in organelle acidification and V-
3 ATPase activity is regulated by reversible disassembly in many different settings. Using the yeast
4 *Saccharomyces cerevisiae* as a replicative aging model, we demonstrate that V-ATPases
5 disassemble into their V_1 and V_0 subcomplexes in aging cells, with release of V_1 subunit C
6 (Vma5) from the lysosome-like vacuole into the cytosol. Disassembly is observed after ≥ 5 cell
7 divisions and results in overall vacuole alkalinization. Caloric restriction, an established
8 mechanism for reversing many age-related outcomes, prevents V-ATPase disassembly in older
9 cells and preserves vacuolar pH homeostasis. Reversible disassembly is controlled in part by the
10 activity of two opposing and conserved factors, the RAVE complex and Oxr1. The RAVE
11 complex promotes V-ATPase assembly and a *rav1* Δ mutant shortens replicative lifespan; Oxr1
12 promotes disassembly and an *oxr1* Δ mutation extends lifespan. Importantly, the level of Rav2, a
13 key subunit of the RAVE complex, declines in aged cells. These data indicate that reduced V-
14 ATPase assembly contributes to the loss of lysosome acidification with age, which affects
15 replicative lifespan.

16

17

18

19

20 Keywords: Aging, lysosomes, proton pumps, *Saccharomyces cerevisiae*, caloric restriction

21

22 INTRODUCTION

23 It is well-documented that lysosomal acidification is compromised with age across many
24 organisms (Nixon, 2020). Reduced lysosomal acidification has multiple downstream functional
25 consequences. Lysosomal hydrolases represent a major arm of the cellular proteostatic
26 machinery and operate optimally at the acidic pH, so cargo degradation is compromised at higher
27 pH (Vilchez, Saez, & Dillin, 2014). Lysosomes are the terminal compartment for multiple
28 autophagy pathways, so clearance of autophagic cargoes and recycling of nutrients, both critical
29 in aging cells, is slowed (Hansen, Rubinsztein, & Walker, 2018; Kaushik et al., 2021). Iron and
30 other heavy metals are sequestered and buffered in the acidic lysosomes; loss of sequestration
31 can induce both oxidative stress (Diab & Kane, 2013; Kurz, Terman, Gustafsson, & Brunk,
32 2008) and deficiency in mitochondrial iron-sulfur proteins (Chen et al., 2020). Reduced
33 lysosomal storage can also create toxic imbalances in amino acids such as cysteine that
34 contribute to loss of mitochondrial function (C. E. Hughes et al., 2020). Recent work has
35 highlighted the central role of the lysosome in nutritional signaling and many aspects of this
36 signaling are linked to acidification (Perera & Zoncu, 2016). It is clear that loss of lysosomal
37 acidification can impact many processes associated with age-related functional decline, but the
38 mechanisms behind increases in lysosomal pH are not fully understood.

39 The highly conserved vacuolar H⁺-ATPase (V-ATPase) acidifies the lumen of lysosomes
40 and lysosome-like vacuoles, as well as endosomes and the late Golgi apparatus, in all eukaryotes
41 (Collins & Forgac, 2020). V-ATPases are multi-subunit protein complexes that couple ATP
42 hydrolysis to proton pumping into organelle lumens. The V-ATPase consists of two
43 subcomplexes: a peripheral V₁ subcomplex oriented toward the cytosol that is responsible for
44 ATP hydrolysis connected to a membrane-embedded V₀ subcomplex containing the proton pore.

45 V-ATPase subunit sequences are conserved across eukaryotes and recent V-ATPase structures
46 indicate very strong structural similarity between yeast and mammalian V-ATPases (Oot &
47 Wilkens, 2020).

48 V-ATPase activity is highly regulated and responsive to multiple environmental
49 conditions. Reversible disassembly is a versatile mechanism of V-ATPase regulation that fine-
50 tunes the activity of the proton pump to meet cellular demands (Collins & Forgac, 2020;
51 Jaskolka, Winkley, & Kane, 2021; Wilkens, Khan, Knight, & Oot, 2023). In reversible
52 disassembly, the V_1 subcomplex is released from the V_0 subcomplex inhibiting both ATP
53 hydrolysis and proton pumping (Kane, 1995; Sumner et al., 1995). V_1 subunit C is dissociated
54 from both subcomplexes and also becomes cytosolic during disassembly (Kane, 1995).
55 Disassembly is post-translational and rapidly reversible (Kane, 1995). It was first observed in the
56 yeast *S. cerevisiae* and the tobacco hornworm *M. sexta* upon acute glucose deprivation and was
57 reversed by glucose replenishment (Kane, 1995; Sumner et al., 1995). Since that time, it has
58 become clear that reversible disassembly occurs in many different settings and in response to
59 diverse signals. For example, unlike yeast cells, most mammalian cells appear to promote V-
60 ATPase reassembly under conditions of nutrient deprivation and mTOR inhibition, possibly as a
61 means of promoting lysosomal proteolysis and nutrient recycling (Ratto et al., 2022; Stransky &
62 Forgac, 2015). In neurons, V-ATPases are reversibly disassembled as part of each synaptic
63 vesicle cycle (Bodzeta, Kahms, & Klingauf, 2017). In cardiomyocytes, lipid overload can
64 promote V-ATPase disassembly in endosomes, ultimately contributing to the long-term insulin
65 resistance (Liu et al., 2017). Reversible disassembly of V-ATPases can also be manipulated by
66 both host cells and pathogens to prevent or facilitate infection (Kohio & Adamson, 2013).

67 Several mechanisms for loss of lysosomal acidification with age have been proposed. In
68 yeast, the long-lived plasma membrane proton pump, Pma1, accumulates in mother cells, and it
69 has been proposed that increased proton export through Pma1 disrupts the balance of Pma1 and
70 V-ATPase activities and compromises organelle acidification (Henderson, Hughes, &
71 Gottschling, 2014). Early loss of vacuolar acidification in yeast has been correlated with
72 defective mitochondrial morphology and function. Both the deacidification and mitochondrial
73 morphology phenotypes are suppressed by overexpression of the V-ATPase catalytic subunit,
74 *VMA1*, or an ER-localized assembly factor, *VPH2*, suggesting a possible deficiency in these
75 factors with age (A. L. Hughes & Gottschling, 2012). In *C. elegans*, stability of the *VMA1*
76 transcript is controlled by a microRNA, miR-1, which can globally control lysosomal
77 acidification (Schiffer et al., 2021). In several systems, mRNA expression for one or more V-
78 ATPase subunit genes has been reported to decrease with age (Ghavidel et al., 2018), but in most
79 cases protein levels have not been assessed. All of these mechanisms could contribute to loss of
80 vacuolar/lysosomal acidification. Wilms et al. (Wilms et al., 2017) demonstrated that the mTOR
81 effector Sch9 promotes V-ATPase assembly and extends yeast chronological lifespan.

82 However, despite the importance of reversible disassembly in regulation of V-ATPase
83 activity, V-ATPase assembly state during aging has not been explored extensively. Here we show
84 that V-ATPase assembly does change with age in a yeast replicative aging model. Increased V-
85 ATPase disassembly in older cells is accompanied by decreased vacuolar acidification that does
86 not appear to stem from reduced V-ATPase subunit levels. Instead, we provide evidence that
87 reduced activity of the RAVE (Regulator of H⁺-ATPase of Vacuolar and Endosomal membranes)
88 assembly complex may give rise to net V-ATPase disassembly and increased lysosomal pH with
89 age.

90

91 **RESULTS**

92 *V-ATPases are more disassembled and vacuoles more alkaline after ~5 cell divisions.*

93 Given the evidence that vacuoles and lysosomes are less acidic in older cells, we
94 hypothesized that V-ATPase assembly and activity might also be changing with age. Replicative
95 aging in the yeast *S. cerevisiae* is a widely accepted model for aging (He, Zhou, & Kennedy,
96 2018). Briefly, yeast cells divide asymmetrically with each cell division giving rise to a new,
97 "rejuvenated" daughter cell from an established mother cell. Each cell division leaves a bud scar
98 on the mother, allowing visual assessment of age. The yeast V₁C subunit (Vma5) is released
99 from both V₁ and V₀ during V-ATPase disassembly, so we first visualized Vma5-GFP
100 localization in a mixed age population of cells (Figure 1). (Note that vacuoles are visible as
101 indentations under DIC (differential interference contrast) optics on the left of the images.) In
102 parallel, we monitored replicative age of each cell by staining with calcofluor white, which labels
103 the bud scars on mother cells. As shown in Figure 1a, Vma5-GFP is tightly localized to the
104 vacuolar membrane in cells with few or no bud scars. In contrast, in older cells with more bud
105 scars, Vma5-GFP exhibited a marked decrease in fluorescence at the vacuolar membrane and a
106 notable increase in cytosolic fluorescence. In order to compare Vma5-GFP localization between
107 cells, we quantitated maximum fluorescence from a line scan across each cell. As shown in
108 Figure 1b, the line scan from a young cell has prominent peaks corresponding to the edges of the
109 vacuole with a high maximum fluorescence signal, while the older cells have less prominent
110 peaks. We conducted the same analysis across populations of cells of mixed age, normalized to
111 the maximum fluorescence signal of young cells and binned the results by the number of bud
112 scars. As shown at the left of Figure 1c, young cells, defined as having less than 5 bud scars,
113 displayed Vma5-GFP localization at the vacuolar membrane. However, the normalized

114 maximum fluorescence signal, representative of vacuole localization, decreases significantly in
115 cells with five bud scars or more. This early onset of V-ATPase disassembly aligns with previous
116 reports indicating changes in lysosomal pH early in replicative aging (A. L. Hughes &
117 Gottschling, 2012).

118 Vma5 is a V_1 subunit that bridges the V_1 and V_0 subcomplexes of the V-ATPase. The V_1
119 subcomplex also contains three copies of Vma2, and the V_0 subcomplex contains the largest
120 subunit, Vph1, which comprises part of the proton pore (Figure 2a). Although Vma5 appears to
121 be the subunit that is released most completely from the membrane by reversible disassembly
122 (Tabke et al., 2014), the rest of the V_1 sector also dissociates from the vacuolar membrane. We
123 assessed the cellular distribution of Vma2-GFP, a V_1 subunit, and Vph1-GFP, a V_0 subunit
124 (Figure 2b). As shown in Figure 2b, there was less membrane-bound Vma2-GFP in older cells
125 relative to younger cells as assessed by line scans as in Figure 1. However, vacuolar Vph1-GFP
126 levels were the same between old and young cells (Figure 2c). These results are consistent with
127 disassembly of the V-ATPase as cells age.

128 Although comparable levels of Vph1 at the vacuole suggests that expression of V_0
129 subunits and V_0 assembly are intact, V_1 subunits could become cytosolic because of reduced V_1
130 subunit levels in older cells. To address this question, we isolated populations old and young
131 yeast cells by biotinylating the cell walls in a mixed age population, allowing growth to continue
132 for several generations, and then obtaining "old" cells by biotin-streptavidin affinity
133 chromatography (Jin, Cao, & Liu, 2021). Daughter cells that emerged after biotinylation cannot
134 bind to magnetic streptavidin beads and represent the "young" population. The age distribution
135 was determined by counting bud scars in each population and binning by the number of buds per
136 cell (Figure 2d). When prepared by this method, the population of old cells peaks at 20-24 bud

137 scars, while there was a median value of 0-4 bud scars in the young population. Cell lysates were
138 prepared from each population and analyzed by SDS-PAGE and immunoblotting. As shown in
139 Figures 2e and f, there is no significant difference in the cellular levels of V₁ subunits Vma1,
140 Vma2, and Vma5 between young and old populations. These results indicate that the cytosolic
141 populations of V₁ subunits arise from disassembly of the V-ATPase, rather than inability to
142 assemble because of lack of V-ATPase subunits.

143 Reversible disassembly of V-ATPases is employed in a number of contexts to provide
144 dynamic regulation of the complex in response to changing cellular conditions. Disassembled V₁
145 and V₀ subcomplexes lack ATPase and proton transport activity and ATP-driven proton pumping
146 is restored upon reassembly. In order to test whether the lower levels of assembled V-ATPases in
147 old cells result in reduced capacity for acidification, we measured the response of young and old
148 cells to an acute glucose deprivation (an abrupt shift to 0% glucose), which promotes
149 disassembly of the yeast V-ATPase, followed by readdition of glucose to a 2% final
150 concentration, which promotes reassembly and reactivation of the complex (Kane, 1995).

151 Young and old yeast cells obtained as described above were loaded with the ratiometric
152 pH sensor BCECF-AM (2',7'-Bis-(2-carboxyethyl)-5-(and-6)-carboxyfluorescein acetoxy methyl
153 ester) which localizes to the vacuole in yeast cells (Diakov, Tarsio, & Kane, 2013). Both young
154 and old cells were shifted to medium with no glucose for ~30 minutes. Fluorescence of cell
155 suspensions was then monitored continuously (Figure 3a), and glucose was added at the
156 indicated time. This assay revealed clear age-dependent differences in the vacuolar pH response
157 to glucose stimulation. Young cells exhibit a rapid drop in vacuolar pH upon glucose addition.
158 This drop was previously shown to be V-ATPase-dependent and to correlate with V-ATPase
159 assembly (Martinez-Munoz & Kane, 2008). In old cells, however, there was a smaller pH

160 decrease after glucose addition, indicating a more alkaline vacuole and consistent with the lower
161 levels of V-ATPase assembly observed by microscopy during growth in glucose-replete
162 conditions in Figures 1 and 2. Quantitative analysis of pH at defined time points across
163 biological replicates (Figure 3b) indicates that vacuoles in old cells are significantly more
164 alkaline than their younger counterparts at each of the indicated time points. These results
165 suggest an age-related alteration in vacuolar pH regulation through the inability of V-ATPase to
166 reassemble. As a result, vacuoles in old cells display a more alkaline pH than vacuoles in young
167 cells.

168 *Caloric restriction restores V-ATPase assembly and vacuolar acidification in older cells.*

169 Caloric restriction (CR) is defined as a reduction in caloric intake in the presence of
170 adequate nutrition (Longo & Anderson, 2022). CR promotes both cellular health and longevity.
171 Extensive research, conducted in diverse model organisms ranging from yeast to worms, flies,
172 and rodents, suggests that CR can have significant anti-aging effects and promote overall health
173 (Longo & Anderson, 2022). In the context of the yeast *S. cerevisiae*, adjusting the concentration
174 of glucose in the growth medium from the 2% used above to 0.5% is a common way to induce
175 CR. This treatment does not significantly reduce growth rate over several cell divisions
176 (Supporting information, Figure 1).

177 As shown in Figure 4, CR reverses the V-ATPase disassembly in older cells. Notably, the
178 V₁ subunits Vma5-GFP (Figure 4a) and Vma2-GFP (Figure 4b) are recruited to the vacuolar
179 membrane in both young and old cells, and there is no significant difference in fluorescence at
180 the vacuolar membrane with age. (Fluorescence intensities of Vph1-GFP continue to be similar
181 between old and young cells (Figure 4c).) This reversal suggests that CR extends V-ATPase

182 assembly beyond the replicative age of ≥ 5 bud scars when cells grown in higher glucose begin to
183 show disassembly.

184 We hypothesized that given the improvement in V-ATPase assembly, vacuolar pH in old
185 cells might also be restored. We grew cells under CR conditions, loaded the vacuoles with
186 BCECF-AM and monitored vacuolar pH before and after addition of glucose as described above.
187 Figure 4d demonstrates that the glucose-stimulated decrease in vacuolar pH, which was
188 compromised in older cells grown in 2% glucose (Figure 3), was restored to the level of young
189 cells in cells after growth under CR conditions. This observation indicates that CR has a direct
190 impact on both V-ATPase assembly and vacuolar acidification in aging cells. In addition, it
191 further highlights the potential connection between V-ATPase assembly, vacuolar acidification
192 and aging.

193

194 *Regulators of V-ATPase assembly state affect replicative lifespan.*

195 If reversible disassembly of the V-ATPase plays a central role in aging of yeast cells, we
196 hypothesized that the cellular factors that regulate V-ATPase assembly might also affect
197 replicative lifespan. The RAVE complex plays a crucial role in regulation of the V-ATPase by
198 reversible disassembly (Jaskolka, Winkley, et al., 2021; Seol, Shevchenko, & Deshaies, 2001). It
199 consists of three subunits: Rav1, Rav2, and Skp1. The RAVE complex is required for reassembly
200 of V-ATPase complexes disassembled by glucose deprivation. In mutants lacking Rav1 or Rav2,
201 V-ATPases are predominantly disassembled into V_1 and V_0 subcomplexes and vacuolar
202 acidification is lost (Seol et al., 2001; Smardon, Tarsio, & Kane, 2002). The RAVE complex
203 associates with V_1 subcomplexes in the cytosol. Although V_1 subunit C is also released from the
204 vacuolar membrane, very little is associated with cytosolic RAVE- V_1 (Jaskolka, Tarsio,

205 Smardon, Khan, & Kane, 2021). In contrast, recent studies suggest that Oxr1, a protein originally
206 associated with resistance to oxidative stress, promotes disassembly of V-ATPases (Khan et al.,
207 2022; Khan & Wilkens, 2024; Klossel et al., 2024) suggesting that RAVE and Oxr1 have
208 opposing effects on the assembly state of V-ATPases as diagrammed in Figure 5a.

209 To further explore the functional significance of these assembly regulators in aging cells,
210 we examined the replicative lifespans of deletion mutants lacking Rav1 or Oxr1 (Figure 5b).
211 Replicative lifespan was measured on YEPD, pH 5 plates, conditions that are optimal for growth
212 of *rav1Δ* strains. Deletion of Rav1 shortened replicative lifespan (median 17 cell divisions, n=
213 30) by 26% relative to wild-type cells (median 23 cell divisions, n= 30). In contrast, the deletion
214 of Oxr1 extended replicative lifespan by 47.8% over wild-type (median 34 cell divisions, n=30).
215 These results reinforce the significance of V-ATPase assembly in replicative aging and suggest
216 that RAVE pro-assembly activity (disrupted in the *rav1Δ* mutant) and Oxr1 anti-assembly
217 activity (lost in *oxr1Δ*) may be central determinants of lifespan.

218 Given these results, we asked whether there were differences in levels of RAVE subunits
219 or Oxr1 between young and old cells. We isolated young and old populations of cells containing
220 myc13-tagged Rav1 or Rav2 by biotinylation and streptavidin magnetic separation as described
221 above (Figure 2), then assessed the levels of the tagged proteins in cell lysates. Although there is
222 no significant difference in Rav1-myc13 levels between young and old cells (Figure 6a), we
223 consistently observed a significant decrease in protein levels of Rav2-myc13 in older cells
224 (Figure 6b). We also assessed expression of *RAV2* in young and old cells by quantitative PCR but
225 observed no significant difference in mRNA levels (Figure 6c). Because Rav2 is required for
226 RAVE complex function in promoting V-ATPase assembly (Seol et al., 2001; Smardon et al.,

227 2002), these results suggest that partial loss of RAVE function in old cells could contribute to
228 reduced V-ATPase assembly and replicative aging.

229 To further explore the basis of the extended replicative lifespan in *oxr1Δ* cells, we
230 observed Vma5-GFP localization in a population of *oxr1Δ* cells of mixed age. As shown in
231 Figure 6d, *oxr1Δ* mutants localize Vma5-GFP to the vacuole even in older cells with ≥ 5 bud
232 scars. In order to quantitate this effect, we again binned cells by the number of bud scars as
233 described above, and compared Vma5-GFP localization to localization in young daughter cells
234 (Figure 6e). In contrast to wild-type cells, there is no significant difference in Vma5-GFP
235 localization in the *oxr1Δ* mutant until cells have divided 25 or more times. We also isolated
236 young and old populations from an HA-tagged Oxr1 strain. As shown in Figure 6f, the levels of
237 Oxr1 do not change with age. However, loss of RAVE function could ultimately favor Oxr1-
238 induced disassembly.

239 Intriguingly, these results suggest that the *oxr1Δ* mutation mirrors the effects of CR on V-
240 ATPase assembly and longevity. The results also indicate that direct manipulation of V-ATPase
241 assembly by mutation of critical assembly factors can affect replicative lifespan. Specifically,
242 promoting V-ATPase assembly through the RAVE complex appears to be important for
243 preserving replicative lifespan, while the opposing effects of Oxr1 on the V-ATPase tend to
244 shorten lifespan. We hypothesized that restoration of V-ATPase assembly in older cells grown
245 under CR conditions (Figure 4) might be supported by restoration of Rav2 levels. To test this, we
246 isolated young and old populations from Rav2-myc13 tagged cells grown under CR conditions.
247 Under these conditions, V-ATPase assembly and function restored in older cells (Figure 4) and as
248 shown in Figure 6g, Rav2 levels are also restored.

249

250 **DISCUSSION**

251 The results described here establish V-ATPase disassembly as an important factor in the
252 reduced vacuolar acidification observed in aging yeast cells. We demonstrate an increase in V-
253 ATPase disassembly at relatively early replicative ages (5-9 cell divisions) similar to the age at
254 which Hughes and Gottschling first observed compromised vacuolar acidification (A. L. Hughes
255 & Gottschling, 2012). We show that promoting assembly of the V-ATPase through CR can
256 restore V-ATPase assembly and vacuolar pH in older cells and that deletion of *Oxr1*, a negative
257 regulator of V-ATPase assembly, can extend replicative lifespan. Taken together, these data
258 support V-ATPase disassembly as a significant age-related factor behind reduced vacuolar and
259 lysosomal acidification and the associated declines in function. This mechanism does not
260 necessarily conflict with those proposed previously. If V-ATPases are more disassembled in older
261 cells, cells may be even less able to tolerate an imbalance between *Pma1* activity at the plasma
262 membrane and V-ATPase activity at the vacuole (Henderson et al., 2014). We see no difference
263 in protein levels of the core V_1 subunits *Vma1* and *Vma2*, or *Vma5*, between young and old
264 cells. The presence of similar levels of *Vph1* in vacuoles of young and old cells suggests that V_0
265 subunits are also expressed at similar levels, since V_0 assembly occurs in the ER and reduced
266 levels of any V_0 subunit reduces V_0 subcomplex levels at the vacuole (Kane, Kuehn, Howald-
267 Stevenson, & Stevens, 1992). The data presented here suggest a post-transcriptional regulatory
268 mechanism, but increased levels of a V_0 assembly factor like *Vph2* (A. L. Hughes & Gottschling,
269 2012) might still promote assembly and improve acidification.

270 Many questions remain to be investigated in the future. The reduction in *Rav2* protein
271 levels with aging appears to be post-transcriptional but we do not yet know whether this arises
272 from reduced translation or increased degradation of the protein. Perhaps more importantly, even

273 though reduced levels of Rav2 levels could help explain increased V-ATPase disassembly, we do
274 not know whether the Rav2 reduction occurs as a result of some general vulnerability in aging
275 cells or is deliberately programmed (Gladyshev et al., 2021). The significant increase in lifespan
276 and prolonged V-ATPase assembly in *oxr1* Δ cells seems to argue against any growth advantage
277 from increased V-ATPase disassembly in older cells, at least at the single cell level.

278 Many aging pathways are tightly linked to nutritional signaling, and reversible
279 disassembly is often driven by nutritional signaling pathways. Given the rapid disassembly of the
280 V-ATPase upon acute glucose deprivation (Kane, 1995), it was initially surprising that growth
281 under CR conditions suppresses V-ATPase disassembly with age. However, we previously
282 showed that the acute disassembly response required glucose concentrations well below 0.5%
283 (Parra & Kane, 1998). In mammalian cells, V-ATPase assembly generally increases in response
284 to nutrient deprivation (Ratto et al., 2022; Stransky & Forgac, 2015). CR could mimic this effect
285 in aging cells, preserving lysosomal acidification and function. Signals involved in reversible
286 disassembly of the V-ATPase are incompletely understood. However, it is intriguing that in yeast,
287 RAVE appears to play a central role in glucose signaling during acute glucose deprivation.
288 RAVE is released from the vacuolar membrane upon acute glucose deprivation and recruited
289 back to the membrane upon glucose restoration, even in the absence of V₁ subunit C and the V₁
290 subcomplex (Jaskolka, Winkley, et al., 2021). The RAVE complex appears to be a major
291 determinant of V-ATPase assembly state in multiple situations, including aging.

292 Reduced V-ATPase assembly could certainly be a factor in the age-related decline in
293 lysosomal acidification and function in higher eukaryotes. Reversible disassembly actively
294 occurs in higher eukaryotes including mammalian cells, so the apparatus for age-induced
295 assembly regulation is available. Rabconnectin-3 complexes of higher eukaryotes are the

296 functional homologues of the yeast RAVE complex (Ratto et al., 2022; Yan, Deneff, &
297 Schupbach, 2009). Oxr1 belongs to a family of TLDC proteins that are also found in mammals,
298 and several of these proteins have been shown to bind to mammalian V-ATPases (Eaton, Brown,
299 & Merkulova, 2021; Wilkens et al., 2023). These data suggest that the core elements for
300 controlled V-ATPase disassembly during aging are present in other cells. Here, we observed V-
301 ATPase disassembly in a yeast replicative aging model, which is most comparable to mammalian
302 cell types that continue to divide, such as adult stem cells (He et al., 2018). However, V-ATPase
303 activity is also critical in the yeast chronological aging model, which is more analogous to long-
304 lived, non-dividing mammalian cells. In this model increased V-ATPase assembly has been
305 associated with longevity (Wilms et al., 2017). Taken together, these data suggest that V-ATPase
306 assembly state is linked to multiple aging models and could easily play a role in aging in higher
307 eukaryotes.

308

309 **METHODS**

310 Yeast strains and plasmids

311 All strains analyzed were in the BY4741 (*MATa his3Δ1 leu2Δ0 met15Δ0 ura3Δ0*) or BY4742
312 (*MATa his3Δ1 leu2Δ0 lys1Δ ura3Δ0*) background. BY4742 strains containing *Vma5-GFP::HIS3*
313 and *Vph1-GFP::HIS3* were constructed as part of the genome-wide GFP-tagging project (Huh et
314 al., 2003) and purchased from Thermo Fisher. *VMA2* was C-terminally tagged with GFP by PCR
315 amplification from pFA6a-GFP-KanMX6 and genomic integration (Longtine et al., 1998). The
316 strain containing *oxr1Δ::kanMX* and *Vma5-GFP::HIS3* was obtained by crossing BY4741
317 *oxr1Δ::kanMX* from the haploid deletion collection and BY4742 *Vma5-GFP::HIS3*, sporulating
318 the diploid, and obtaining spores with the desired genotype by tetrad dissection. The pRS316

319 Oxr1-HA plasmid (Khan & Wilkens, 2024) was transformed into *oxr1Δ* and transformants were
320 selected for on SC medium (fully supplemented minimal medium) lacking uracil. Rav1-
321 myc13::*kanMX* and Rav2-myc13::*kanMX* strains were described previously (Smardon et al.,
322 2002). The tagged alleles were PCR amplified from the original strains and integrated into
323 BY4741.

324 Fluorescence microscopy

325 Strains expressing GFP-tagged Vma5, Vma2, or Vph1 were grown to log phase in SC
326 medium containing either 2% or 0.5% glucose overnight, pelleted by centrifugation, then
327 suspended in fresh medium containing 2% or 0.5% glucose and grown for an additional 2 hours.
328 Cells were stained with calcofluor white (CW) by diluting a 1 mg/ml CW stock to a final
329 concentration of 10 µg/ml with cells, 5 min prior to imaging. Cells were visualized with a 100x
330 oil (NA 1.4) objective on a Zeiss Imager.Z1 fluorescence microscope with a Hamamastu CCD
331 camera and AxioVision software. Cells were viewed through differential interference contrast
332 (DIC) optics or fluorescence was visualized using a DAPI filter set for CW and a GFP filter set
333 for GFP-tagged subunits. Bud scars were counted from CW staining; in mixed age populations,
334 cells with 5 or more bud scars were designated as old and those with less than 5 as young. To
335 obtain a more precise count of bud scars for binning, cells were visualized on multiple focal
336 planes. GFP fluorescence was then determined for each of the binned ranges. Images of GFP-
337 tagged proteins were captured then processed in FIJI. To assess vacuolar localization, a line was
338 drawn across a cell and through the vacuolar membrane. From this line scan, a plot illustrating
339 fluorescence intensity along the line was generated, with peaks indicating areas of elevated
340 fluorescence at the vacuolar membrane. By quantifying the peak intensity (maximum
341 fluorescence), we quantitated the vacuolar localization for each GFP-tagged subunit. Each

342 biological replicate corresponds to a distinct culture of yeast cells. Maximum fluorescence was
343 quantitated for at least 20 young and 20 old cells per biological replicate. When cells were
344 binned by age, at least 20 cells per biological replicate were counted for each bin. To normalize
345 maximum fluorescence across replicates, the maximum fluorescence from line scans of young
346 and old cells in each biological replicate was averaged and then divided by the average of the
347 young cells in that replicate. The normalized fluorescence for each biological replicate was
348 plotted, along with average intensities across replicates \pm s.e.m. (standard error of the mean).
349 Statistical significance was determined by t-test for the young and old cell comparisons and by
350 ANOVA for the binned samples. In order to show the range of values for the young cells across
351 experiments, the values for the young cells in each biological replicate were averaged and the
352 values for the individual replicates were divided by the average and shown as points on each
353 graph.

354 *Age Enrichment*

355 Age enrichment was performed as described by Jin et al. (Jin et al., 2021). Cells were collected
356 from a 50 mL fresh overnight culture in YEP (yeast extract-peptone medium) supplemented with
357 2% or 0.5% glucose to an OD₆₀₀ of 1.0 and washed twice with cold phosphate-buffered saline
358 (PBS), pH 7.4. Cells were pelleted by centrifugation and washed three times in cold sterile PBS,
359 then labeled with 1.6 mg/ml EZ-Link Sulfo-NHS-LC-Biotin (Pierce) at room temperature for 30
360 min with gentle agitation. After labeling, the cells were washed three times with cold PBS, pH
361 8.0, to remove free biotin, and resuspended in YEP supplemented with 2% or 0.5% glucose for
362 growth overnight. After 16 hours, cells were pelleted by centrifugation and resuspended in 35 ml
363 of cold PBS, pH 7.4, mixed with 250 μ l of a magnetic streptavidin bead suspension (Pierce), and
364 incubated for 60 min at 4°C. The mixture, in a 50 mL conical tube, was loaded onto a magnetic

365 separation column (Permagen) at 4°C to separate biotinylated cells and allow unbound cells to
366 settle, and supernatant was removed gently by pipetting. Magnetically separated cells were
367 subsequently washed three times by resuspending in 35 mL PBS, pH 7.4 supplemented with 2%
368 or 0.5% glucose, repeating magnetic separation, and discarding the supernatant. After washing,
369 cells were resuspended in 200 mL of YEP or SC supplemented with 2% or 0.5% glucose and
370 allowed to grow for an additional 4 hours before obtaining the final "old" mother cells and
371 "young" daughter cells. Cells were loaded on the magnetic separation column as described above
372 and daughter cells obtained from the supernatant were pelleted by centrifugation to obtain a
373 concentrated population of young cells. After the final wash, the magnetic beads were
374 resuspended in 1 ml PBS 7.4 and centrifuged at 4000g to concentrate the old population. The two
375 populations were then stored at -80°C for further biochemical analysis or used immediately for
376 pH measurements (see below).

377 Whole Cell Lysates and Immunoblots

378 Cell pellets from age-enriched young and old cell populations were resuspended in hot
379 cracking buffer (8 M urea, 5% SDS, 1 mM EDTA, 50 mM Tris-HCl, pH 6.8) and glass beads.
380 The mixture was vortexed for 10 sec and incubated at 95 °C for 30 sec repeatedly for a total of 5
381 min. Cellular debris was pelleted by centrifugation at 16,000 × g for 2 min, and supernatants
382 containing whole-cell extracts were used immediately or stored at -80 °C until use.

383 After determination of protein concentrations by Bradford assay, equal concentrations of
384 protein for each sample were separated by SDS-PAGE and transferred to a nitrocellulose
385 membrane. Blots were blocked for 1 hr in TBST (20 mM Tris-HCl pH 7.5, 150 mM NaCl,
386 0.05% Tween-20) plus 5% nonfat milk before incubating overnight with primary antibodies at 4
387 °C with agitation. Primary antibodies (all used at a 1:500 dilution) included mouse monoclonal

388 antibodies: 7A2 against Vma5, 10D7 against Vph1, 8B1 against Vma1, and 13D11 against Vma2
389 (Kane et al., 1992). In addition, anti-myc monoclonal 9E10 (Santa Cruz Biotechnology), anti-HA
390 monoclonal (BioLegend), and anti-GAPDH (Proteintech) antibodies were purchased and used at
391 1:500, 1:500, and 1:10000, respectively. After washing three times with TBST buffer, HRP-
392 conjugated anti-mouse secondary antibody (Bio-Rad) was added at a final dilution of 1:2000 and
393 incubated for 60 min at room temperature. The blot was washed again, incubated with Bio-Rad
394 Clarity Western ECL substrate and imaged in an Azure Sapphire FL Biomolecular Imager.
395 Images were quantified using FIJI. Molecular mass markers were included on every blot. In
396 images of blots, the mass of the marker nearest in size to the protein is indicated.

397 Vacuolar pH Measurements

398 Vacuolar pH was measured using the ratiometric fluorescent dye BCECF-AM (Invitrogen) as
399 described previously (Diakov et al., 2013). Age-enriched populations of cells were loaded with
400 BCECF-AM in YEP supplemented with 2% or 0.5% glucose. After washing with YEP media to
401 remove dye, cells were resuspended in YEP, deprived of glucose, and incubated on rotator for 30
402 min. For fluorescence measurement, 20 μ l of cell suspension was diluted into 3 ml 1 mM MES
403 pH 5.0 buffer, and fluorescence intensity at excitation wavelengths 450 and 495 nm and emission
404 wavelength 535 nm and was monitored continuously in a Horiba Jovin Yvon Spectrafluor Max
405 fluorometer with temperature maintained at 30°C. The fluorescence ratio for each sample was
406 calibrated for each strain in every experiment by clamping the pH to a range of values from 5.0
407 to 7.0 as described, and the resulting calibration curve was used to convert the experimental
408 fluorescence ratios to vacuolar pH.

409 Replicative Life Span

410 Replicative life span assays were performed on YEP, 2% glucose plates buffered to pH 5.
411 Daughter cells were sequentially removed by micromanipulation (Steffen, Kennedy, &
412 Kaeberlein, 2009). Survival curves are pooled data from experiment-matched controls. The
413 number of divisions for 30 mother cells were scored for each curve. p values for replicative life
414 span survival curve comparisons were calculated with a Cox regression model. Kaplan-Meier
415 survival curves were plotted with GraphPad Prism.

416 *RT-PCR of RAV2 from young and old cells*

417 RNA was extracted from young and old cells, obtained by age enrichment as described above,
418 using the NEB Monarch Total RNA Miniprep Kit . RT-PCR was conducted using the NEB Luna
419 Universal One-Step RT-qPCR Kit and performed on a Bio-Rad CFX384 Touch System. Data
420 analysis was conducted using CFX Maestro Software to determine expression levels.

421

422 **Acknowledgements:** This work was supported by NIH R35 GM145256 to P.M.K. The authors
423 thank M. Murad Khan and Dr. Stephan Wilkens for sharing the *oxr1*Δ strain and Oxr1-HA
424 plasmid, and Dr. Xin Jie Chen for helpful discussions and a critical reading of the manuscript.

425 **Author contributions:** F.H. performed experiments, analyzed data, prepared figures, and wrote
426 the first draft of the manuscript; P.M.K. obtained funding for the project, analyzed data, prepared
427 figures, and contributed to writing of the manuscript.

428 **Conflict of interest:** The authors declare that they have no conflicts of interest with the contents
429 of this article.

430 **Data availability:** The data that support the findings of this study are openly available in
431 Upstate.figshare.com at <https://upstate.figshare.com>. DOI: 10.58120/upstate.26023660

432

523 **REFERENCES**

- 524
- 525 Bodzeta, A., Kahms, M., & Klingauf, J. (2017). The Presynaptic v-ATPase Reversibly
526 Disassembles and Thereby Modulates Exocytosis but Is Not Part of the Fusion Machinery.
527 *Cell Rep*, 20(6), 1348-1359. doi:10.1016/j.celrep.2017.07.040
- 528 Chen, K. L., Ven, T. N., Crane, M. M., Brunner, M. L. C., Pun, A. K., Helget, K. L., . . . Wasko, B.
529 M. (2020). Loss of vacuolar acidity results in iron-sulfur cluster defects and divergent
530 homeostatic responses during aging in *Saccharomyces cerevisiae*. *Geroscience*, 42(2), 749-
531 764. doi:10.1007/s11357-020-00159-3
- 532 Collins, M. P., & Forgac, M. (2020). Regulation and function of V-ATPases in physiology and
533 disease. *Biochim Biophys Acta Biomembr*, 1862(12), 183341.
534 doi:10.1016/j.bbamem.2020.183341
- 535 Diab, H. I., & Kane, P. M. (2013). Loss of vacuolar H⁺-ATPase (V-ATPase) activity in yeast
536 generates an iron deprivation signal that is moderated by induction of the peroxiredoxin
537 TSA2. *Journal of Biological Chemistry*, 288(16), 11366-11377. doi:M112.419259 [pii]
538 10.1074/jbc.M112.419259
- 539 Diakov, T. T., Tarsio, M., & Kane, P. M. (2013). Measurement of vacuolar and cytosolic pH in
540 vivo in yeast cell suspensions. *J Vis Exp, Apr* 19(74). doi:10.3791/50261
- 541 Eaton, A. F., Brown, D., & Merkulova, M. (2021). The evolutionary conserved TLDc domain
542 defines a new class of (H(+))V-ATPase interacting proteins. *Sci Rep*, 11(1), 22654.
543 doi:10.1038/s41598-021-01809-y
- 544 Ghavidel, A., Baxi, K., Prusinkiewicz, M., Swan, C., Belak, Z. R., Eskiw, C. H., . . . Harkness, T.
545 A. (2018). Rapid Nuclear Exclusion of Hcm1 in Aging *Saccharomyces cerevisiae* Leads to
546 Vacuolar Alkalinization and Replicative Senescence. *G3 (Bethesda)*, 8(5), 1579-1592.
547 doi:10.1534/g3.118.200161
- 548 Gladyshev, V. N., Kritchevsky, S. B., Clarke, S. G., Cuervo, A. M., Fiehn, O., de Magalhaes, J. P.,
549 . . . Cummings, S. R. (2021). Molecular Damage in Aging. *Nat Aging*, 1(12), 1096-1106.
550 doi:10.1038/s43587-021-00150-3
- 551 Hansen, M., Rubinsztein, D. C., & Walker, D. W. (2018). Autophagy as a promoter of longevity:
552 insights from model organisms. *Nat Rev Mol Cell Biol*, 19(9), 579-593.
553 doi:10.1038/s41580-018-0033-y
- 554 He, C., Zhou, C., & Kennedy, B. K. (2018). The yeast replicative aging model. *Biochim Biophys*
555 *Acta Mol Basis Dis*, 1864(9 Pt A), 2690-2696. doi:10.1016/j.bbadis.2018.02.023
- 556 Henderson, K. A., Hughes, A. L., & Gottschling, D. E. (2014). Mother-daughter asymmetry of pH
557 underlies aging and rejuvenation in yeast. *Elife*, 3, e03504. doi:10.7554/eLife.03504
- 558 Hughes, A. L., & Gottschling, D. E. (2012). An early age increase in vacuolar pH limits
559 mitochondrial function and lifespan in yeast. *Nature*, 492(7428), 261-265. doi:nature11654
560 [pii]
561 10.1038/nature11654
- 562 Hughes, C. E., Coody, T. K., Jeong, M. Y., Berg, J. A., Winge, D. R., & Hughes, A. L. (2020).
563 Cysteine Toxicity Drives Age-Related Mitochondrial Decline by Altering Iron
564 Homeostasis. *Cell*, 180(2), 296-310 e218. doi:10.1016/j.cell.2019.12.035
- 565 Huh, W. K., Falvo, J. V., Gerke, L. C., Carroll, A. S., Howson, R. W., Weissman, J. S., & O'Shea,
566 E. K. (2003). Global analysis of protein localization in budding yeast. *Nature*, 425(6959),
567 686-691. Retrieved from

- 568 http://www.ncbi.nlm.nih.gov/entrez/query.fcgi?cmd=Retrieve&db=PubMed&dopt=Citation&list_uids=14562095
569
- 570 Jaskolka, M. C., Tarsio, M., Smardon, A. M., Khan, M. M., & Kane, P. M. (2021). Defining steps
571 in RAVE-catalyzed V-ATPase assembly using purified RAVE and V-ATPase
572 subcomplexes. *J Biol Chem*, 296, 100703. doi:10.1016/j.jbc.2021.100703
- 573 Jaskolka, M. C., Winkley, S. R., & Kane, P. M. (2021). RAVE and Rabconnectin-3 Complexes as
574 Signal Dependent Regulators of Organelle Acidification. *Front Cell Dev Biol*, 9, 698190.
575 doi:10.3389/fcell.2021.698190
- 576 Jin, X., Cao, X., & Liu, B. (2021). Isolation of Aged Yeast Cells Using Biotin-Streptavidin Affinity
577 Purification. *Methods Mol Biol*, 2196, 223-228. doi:10.1007/978-1-0716-0868-5_17
- 578 Kane, P. M. (1995). Disassembly and reassembly of the yeast vacuolar H(+)-ATPase in vivo. *J*
579 *Biol Chem*, 270(28), 17025-17032.
- 580 Kane, P. M., Kuehn, M. C., Howald-Stevenson, I., & Stevens, T. H. (1992). Assembly and targeting
581 of peripheral and integral membrane subunits of the yeast vacuolar H(+)-ATPase. *J Biol*
582 *Chem*, 267(1), 447-454.
- 583 Kaushik, S., Tasset, I., Arias, E., Pampliega, O., Wong, E., Martinez-Vicente, M., & Cuervo, A. M.
584 (2021). Autophagy and the hallmarks of aging. *Ageing Res Rev*, 72, 101468.
585 doi:10.1016/j.arr.2021.101468
- 586 Khan, M. M., Lee, S., Couoh-Cardel, S., Oot, R. A., Kim, H., Wilkens, S., & Roh, S. H. (2022).
587 Oxidative stress protein Oxr1 promotes V-ATPase holoenzyme disassembly in catalytic
588 activity-independent manner. *EMBO J*, 41(3), e109360. doi:10.15252/embj.2021109360
- 589 Khan, M. M., & Wilkens, S. (2024). Molecular mechanism of Oxr1p mediated disassembly of
590 yeast V-ATPase. *EMBO Rep*. doi:10.1038/s44319-024-00126-5
- 591 Klossel, S., Zhu, Y., Amado, L., Bisinski, D. D., Ruta, J., Liu, F., & Gonzalez Montoro, A. (2024).
592 Yeast TLDC domain proteins regulate assembly state and subcellular localization of the V-
593 ATPase. *EMBO J*. doi:10.1038/s44318-024-00097-2
- 594 Kohio, H. P., & Adamson, A. L. (2013). Glycolytic control of vacuolar-type ATPase activity: a
595 mechanism to regulate influenza viral infection. *Virology*, 444(1-2), 301-309. doi:S0042-
596 6822(13)00396-6 [pii]
597 10.1016/j.virol.2013.06.026
- 598 Kurz, T., Terman, A., Gustafsson, B., & Brunk, U. T. (2008). Lysosomes in iron metabolism,
599 ageing and apoptosis. *Histochem Cell Biol*, 129(4), 389-406. Retrieved from
600 http://www.ncbi.nlm.nih.gov/entrez/query.fcgi?cmd=Retrieve&db=PubMed&dopt=Citation&list_uids=18259769
601
- 602 Liu, Y., Steinbusch, L. K. M., Nabben, M., Kapsokalyvas, D., van Zandvoort, M., Schonleitner, P.,
603 . . . Luiken, J. (2017). Palmitate-Induced Vacuolar-Type H(+)-ATPase Inhibition Feeds
604 Forward Into Insulin Resistance and Contractile Dysfunction. *Diabetes*, 66(6), 1521-1534.
605 doi:10.2337/db16-0727
- 606 Longo, V. D., & Anderson, R. M. (2022). Nutrition, longevity and disease: From molecular
607 mechanisms to interventions. *Cell*, 185(9), 1455-1470. doi:10.1016/j.cell.2022.04.002
- 608 Longtine, M. S., McKenzie, A., 3rd, Demarini, D. J., Shah, N. G., Wach, A., Brachat, A., . . .
609 Pringle, J. R. (1998). Additional modules for versatile and economical PCR-based gene
610 deletion and modification in *Saccharomyces cerevisiae*. *Yeast*, 14(10), 953-961.
- 611 Martinez-Munoz, G. A., & Kane, P. (2008). Vacuolar and plasma membrane proton pumps
612 collaborate to achieve cytosolic pH homeostasis in yeast. *J Biol Chem*, 283(29), 20309-
613 20319. doi:M710470200 [pii]

- 614 10.1074/jbc.M710470200
615 Nixon, R. A. (2020). The aging lysosome: An essential catalyst for late-onset neurodegenerative
616 diseases. *Biochim Biophys Acta Proteins Proteom*, 1868(9), 140443.
617 doi:10.1016/j.bbapap.2020.140443
618 Oot, R. A., & Wilkens, S. (2020). A "Sugar-Coated" Proton Pump Comes into Focus: High-
619 Resolution Structure of a Human V-ATPase. *Mol Cell*, 80(3), 379-380.
620 doi:10.1016/j.molcel.2020.10.020
621 Parra, K. J., & Kane, P. M. (1998). Reversible association between the V1 and V0 domains of yeast
622 vacuolar H⁺-ATPase is an unconventional glucose-induced effect. *Mol Cell Biol*, 18(12),
623 7064-7074. Retrieved from <http://mcb.asm.org/cgi/content/full/18/12/7064>
624 Perera, R. M., & Zoncu, R. (2016). The Lysosome as a Regulatory Hub. *Annu Rev Cell Dev Biol*,
625 32, 223-253. doi:10.1146/annurev-cellbio-111315-125125
626 Ratto, E., Chowdhury, S. R., Siefert, N. S., Schneider, M., Wittmann, M., Helm, D., & Palm, W.
627 (2022). Direct control of lysosomal catabolic activity by mTORC1 through regulation of
628 V-ATPase assembly. *Nat Commun*, 13(1), 4848. doi:10.1038/s41467-022-32515-6
629 Schiffer, I., Gerisch, B., Kawamura, K., Laboy, R., Hewitt, J., Denzel, M. S., . . . Antebi, A. (2021).
630 miR-1 coordinately regulates lysosomal v-ATPase and biogenesis to impact proteotoxicity
631 and muscle function during aging. *Elife*, 10. doi:10.7554/eLife.66768
632 Seol, J. H., Shevchenko, A., & Deshaies, R. J. (2001). Skp1 forms multiple protein complexes,
633 including RAVE, a regulator of V-ATPase assembly. *Nat Cell Biol*, 3(4), 384-391.
634 Smardon, A. M., Tarsio, M., & Kane, P. M. (2002). The RAVE complex is essential for stable
635 assembly of the yeast V-ATPase. *J Biol Chem*, 277(16), 13831-13839.
636 Steffen, K. K., Kennedy, B. K., & Kaerberlein, M. (2009). Measuring replicative life span in the
637 budding yeast. *J Vis Exp*(28). doi:10.3791/1209
638 Stransky, L. A., & Forgac, M. (2015). Amino Acid Availability Modulates Vacuolar H⁺-ATPase
639 Assembly. *Journal of Biological Chemistry*, 290(45), 27360-27369. doi:M115.659128 [pii]
640 10.1074/jbc.M115.659128
641 Sumner, J. P., Dow, J. A., Earley, F. G., Klein, U., Jager, D., & Wieczorek, H. (1995). Regulation
642 of plasma membrane V-ATPase activity by dissociation of peripheral subunits. *J Biol*
643 *Chem*, 270(10), 5649-5653.
644 Tabke, K., Albertmelcher, A., Vitavska, O., Huss, M., Schmitz, H. P., & Wieczorek, H. (2014).
645 Reversible disassembly of the yeast V-ATPase revisited under in vivo conditions.
646 *Biochemical Journal*, 462(1), 185-197. doi:BJ20131293 [pii]
647 10.1042/BJ20131293
648 Vilchez, D., Saez, I., & Dillin, A. (2014). The role of protein clearance mechanisms in organismal
649 ageing and age-related diseases. *Nat Commun*, 5, 5659. doi:10.1038/ncomms6659
650 Wilkens, S., Khan, M. M., Knight, K., & Oot, R. A. (2023). Tender love and disassembly: How a
651 TLDC domain protein breaks the V-ATPase. *Bioessays*, 45(7), e2200251.
652 doi:10.1002/bies.202200251
653 Wilms, T., Swinnen, E., Eskes, E., Dolz-Edo, L., Uwineza, A., Van Essche, R., . . . Winderickx, J.
654 (2017). The yeast protein kinase Sch9 adjusts V-ATPase assembly/disassembly to control
655 pH homeostasis and longevity in response to glucose availability. *PLoS Genet*, 13(6),
656 e1006835. doi:10.1371/journal.pgen.1006835
657 Yan, Y., Denef, N., & Schupbach, T. (2009). The vacuolar proton pump, V-ATPase, is required for
658 notch signaling and endosomal trafficking in Drosophila. *Dev Cell*, 17(3), 387-402.
659 doi:S1534-5807(09)00260-3 [pii]

660 10.1016/j.devcel.2009.07.001
661

433 **FIGURE LEGENDS**

434 **Figure 1: V-ATPases are more disassembled in yeast cells of older replicative age. (a)**

435 BY4742 cells expressing Vma5-GFP grown in SC containing 2% glucose. Differential
436 interference contrast microscopy (DIC) was used to visualize vacuoles. Bud scars are stained
437 with calcofluor white (CW) to determine replicative age. **(b)** Left panel provides representative
438 example of quantitative measurements using line scans. The young cell is from the dashed white
439 box in the Vma5-GFP image of **Figure 1a** and the old cell is from the dashed red box. Plot
440 profiles are superimposed for the young cell (black) and old cell (red). **(c)** Quantitation of
441 maximum fluorescent intensity across five biological replicates, after normalization to the
442 average intensity in the youngest bin for each replicate. Each biological replicate (dot) represents
443 at least 20 cells and bars represent the mean +/- s.e.m. Significance was calculated by ordinary
444 one-way ANOVA. “Old” for subsequent experiments (without age enrichment) is categorized at
445 ≥ 5 bud scars. **** represents a p-value < 0.0001 .

446

447 **Figure 2: Age-enriched populations of cells have comparable levels of V-ATPase subunits.**

448 **(a)** Diagram of V-ATPase showing the relative positions of Vma5, Vma2, and Vph1 (Image was
449 prepared with Biorender.com). **(b)** BY4742 cells expressing Vma2-GFP (V₁B) grow in SC with
450 2% glucose. CW was used to visualize bud scars. The CW images for young cells were
451 overexposed relative to those for the old cells in order to visualize the low level staining in cells
452 with few bud scars. Normalized maximum fluorescence was obtained through line scan
453 quantitation using FIJI as in **Figure 1**. Means +/- s.e.m. of three biological replicates are shown;
454 each replicate is represented by a dot. Significance was calculated by unpaired Student's *t* test,
455 *** p value=0.0009 . **(c)** Cells expressing Vph1-GFP were visualized and analyzed as described

456 in **2b. (d)** After biotin-streptavidin age enrichment, bud scars were counted for 100 cells in
457 young and old populations, binned by bud count, and the age distribution plotted. **(e)** Lysates
458 were prepared from age-enriched populations defined as in **1c** and equal protein concentrations
459 were separated by SDS-PAGE and examined by immunoblot for V-ATPase protein levels in
460 young (Y) vs. old (O) cell populations defined as in **1c. (f)** Band intensities were quantified using
461 FIJI, ratios of V-ATPase subunit levels to the GAPDH internal control were calculated, and ratios
462 were normalized to the young population for each biological replicate. Significance calculated by
463 unpaired Student's *t* test. Data are presented as mean (horizontal bars) \pm s.e.m. (whiskers) of
464 three biological replicates. n.s.= not significant.

465

466 **Figure 3: Vacuolar pH is more alkaline in old cells. (a)** Vacuolar pH responses were measured
467 for wild-type BY4742 age-enriched young and old populations as described in Methods.
468 Glucose-deprived cultures were loaded with BCECF-AM. Fluorescence intensity values were
469 collected every 10 sec at excitation wavelengths 450 and 490 nm and emission wavelength 535
470 nm, and glucose was added to a final concentration of 2% after 3 min. The ratio of fluorescence
471 signals from the two excitation wavelengths was calculated and converted to pH via a calibration
472 curve. **(b)** Fluorescence measurements at 1 min. (before glucose addition), 5 min (2 min. after
473 glucose addition), and 8 min. (5 min after glucose addition). Calculated pH measurements are
474 presented as mean (horizontal bars) \pm s.e.m. (whiskers) of three biological replicates. * indicates
475 a p value of 0.02, ** represents a p value of 0.001.

476

477 **Figure 4: Caloric restriction (0.5% glucose) restores V-ATPase assembly and vacuolar pH**
478 **in old cells. (a), (b), (c)** Strains used in **Figures 1** and **2** show recruitment of Vma5-GFP **4a** and

479 Vma2-GFP **4b** to the vacuolar membrane after growth in SC with 0.5% glucose while Vph1-GFP
480 **4c** remains unchanged. Maximum fluorescence was measured and normalized as described in
481 Methods and **Figure 1**. CW was visualized in young and old cells as described in **Figure 2b**. No
482 significant differences between young and old cells was observed as calculated by unpaired
483 Student's *t* test. **(d)** Young and old cell populations were obtained by biotin-streptavidin age-
484 enrichment from cells grown in YEP supplemented with 0.5% glucose, and vacuolar pH
485 responses were measured. Data were collected and analyzed as in **Figure 3b**. Quantitated data
486 are presented as mean (horizontal bars) \pm s.e.m. (whiskers) of three biological replicates.

487

488 **Figure 5: Effects of *rav1* Δ and *oxr1* Δ on replicative lifespan. (a)** Schematic of reversible
489 disassembly highlighting the roles of the RAVE complex and Oxr1 (Image was prepared with
490 Biorender.com). **(b)** Kaplan-Meier curves comparing the replicative lifespan (RLS) of *rav1* Δ
491 (green), *oxr1* Δ (red), and wild-type cells (black). Median number of replicative generations is
492 shown in parentheses for each strain, and the difference between *rav1* Δ and *oxr1* Δ median values
493 and wild-type are expressed as %. Deletion of *OXR1* significantly increases yeast RLS
494 ($p < 0.001$), and deletion of RAVE component *RAV1* shortens RLS ($p < 0.01$).

495

496 **Figure 6: Rav2 level is reduced during replicative aging, but restored by CR. (a)** Analysis of
497 Rav1 levels in young and old cells. Age-enriched populations were obtained from BY4741 cells
498 containing Rav1-myc₁₃ (young (Y) versus old (O) cells), and cell lysates were prepared,
499 separated, and quantitated as described in Methods and **Figure 2**. Normalized data are presented
500 as mean (horizontal bars) \pm s.e.m. (whiskers) of three biological replicates. ns=not significant **(b)**
501 Immunoblot analysis of BY4741 Rav2-myc₁₃ from young and old cells prepared as in **6a**.

502 Normalized data are presented as mean (horizontal bars) \pm s.e.m. (whiskers) of three biological
503 replicates. P-value 0.0094. **(c)** Quantitative RT-PCR comparing expression of *RAV2* mRNA
504 between young and old cells. **(d)** Wild-type and *oxr1* Δ cells containing *Vma5*-GFP were grown
505 in SC containing 2% glucose. DIC used to visualize vacuoles and CW used to visualize bud scars
506 as described in **Figure 2b**. **(e)** BY4741 *oxr1* Δ cells were binned by the number of bud scars and
507 normalized maximal fluorescence quantitated as described in **Figure 1**. *** indicates a P value
508 of 0.001 in comparison to the youngest bin; other bins are not significantly different from the
509 youngest bin. **(f)** Immunoblot analysis of a BY4741 *oxr1* Δ strain expressing *Oxr1*-HA from a
510 low copy plasmid. Young and old cell populations were isolated as in **6a**. Data are presented as
511 mean (horizontal bars) \pm s.e.m. (whiskers) of three biological replicates. **(g)** Immunoblot analysis
512 comparing *Rav2*-myc₁₃ levels in cells grown in YEP supplemented with 2% glucose and 0.5%
513 glucose (CR conditions). Samples were prepared and analyzed as in **6b**. Quantification of data
514 are presented as mean (horizontal bars) \pm s.e.m. (whiskers) of three biological replicates. ***
515 indicates a P value of 0.0001, n.s.= not significant.

516

517 **Supporting information, Figure 1: Cells show similar growth rates over 12 hours in 2%**
518 **and 0.5% glucose.** BY4742 cells at log phase were diluted into YEP containing either 2% or
519 0.5% glucose as indicated. OD₆₀₀ was measured every hour for 12 hours.

520

521

522

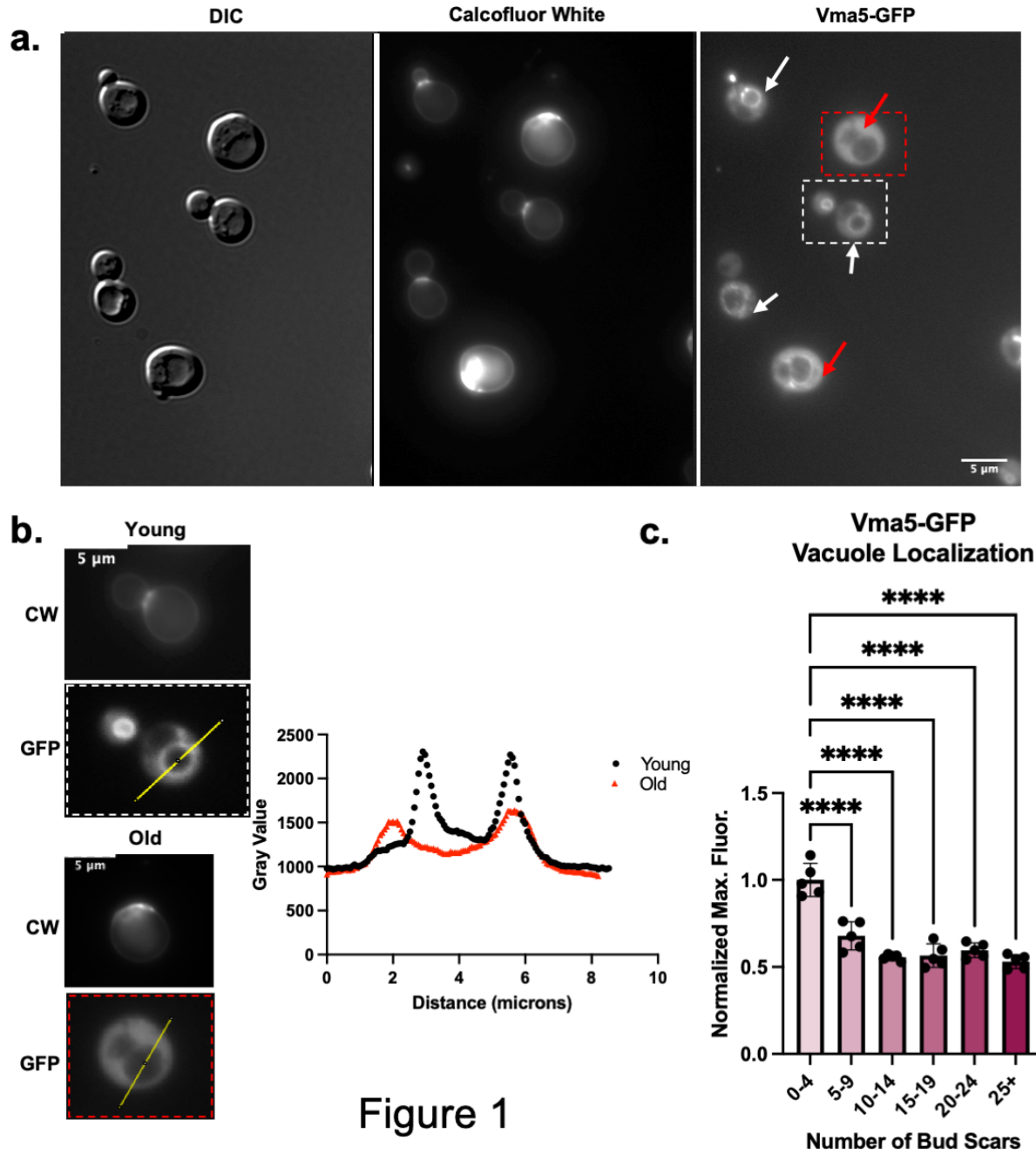


Figure 1

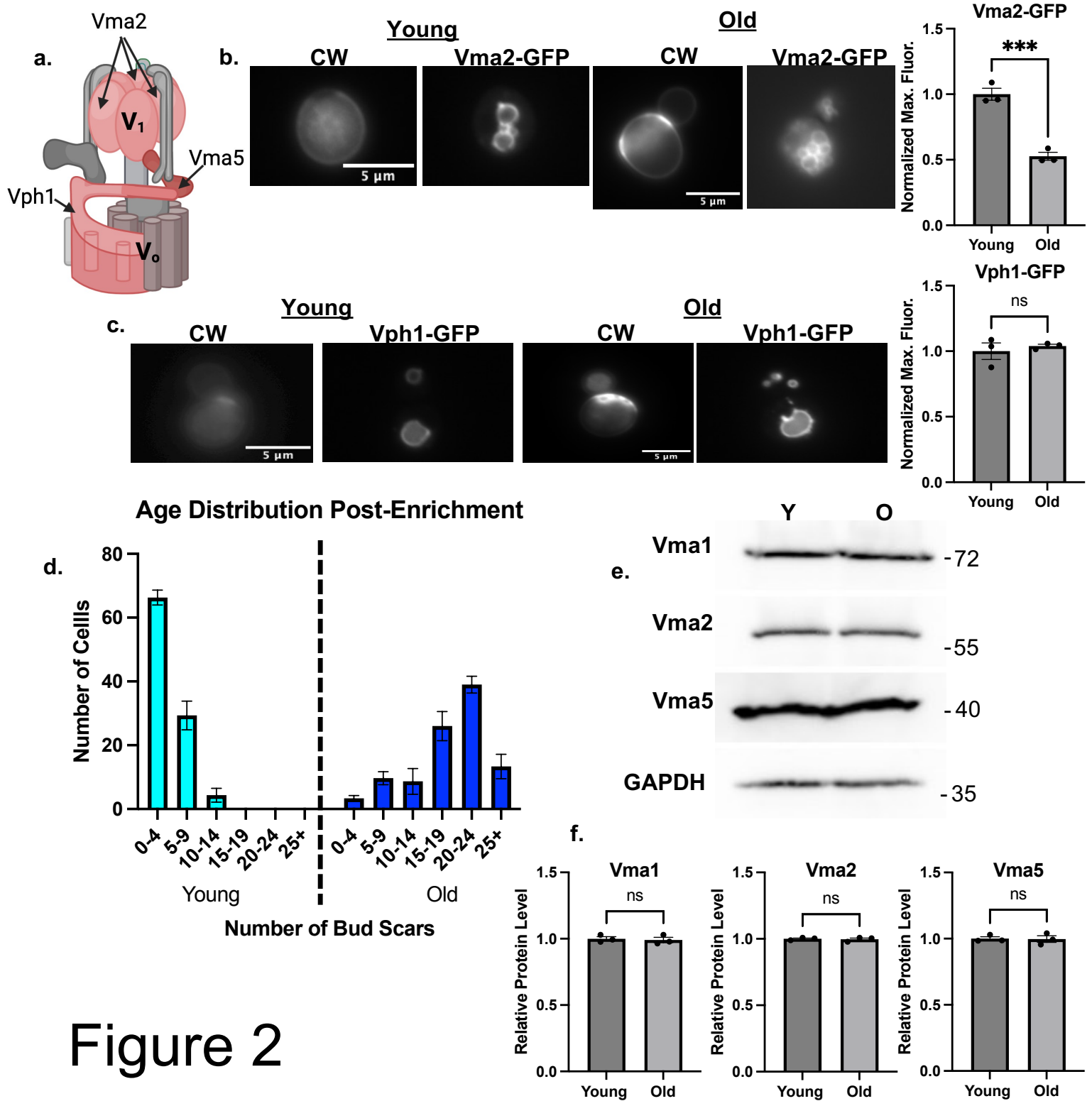


Figure 2

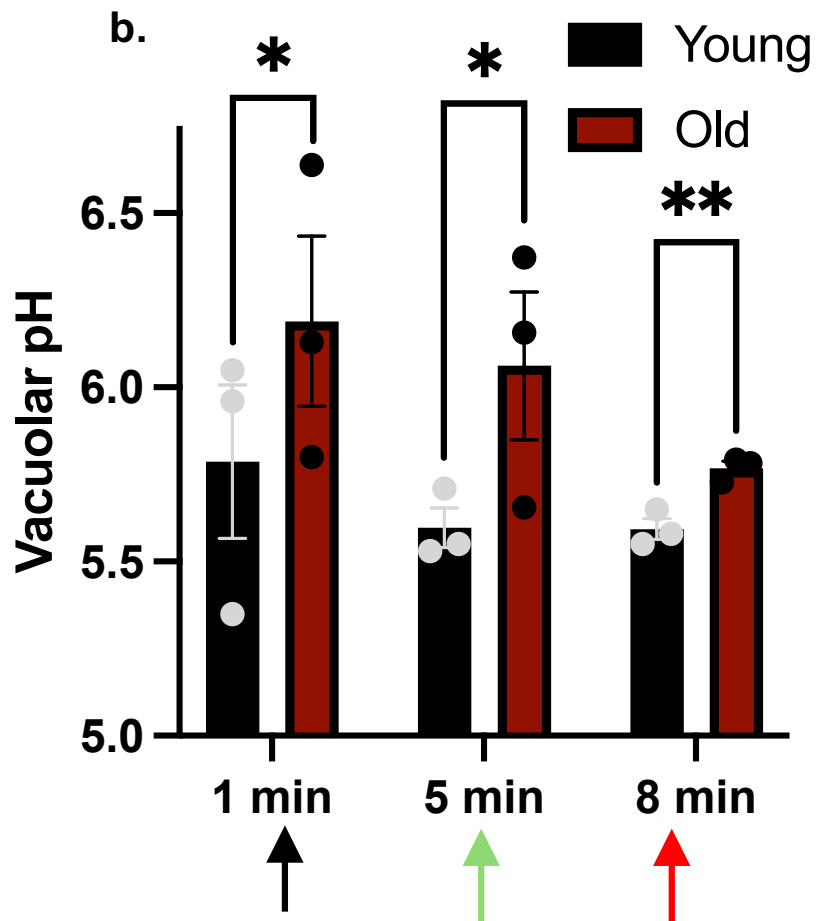
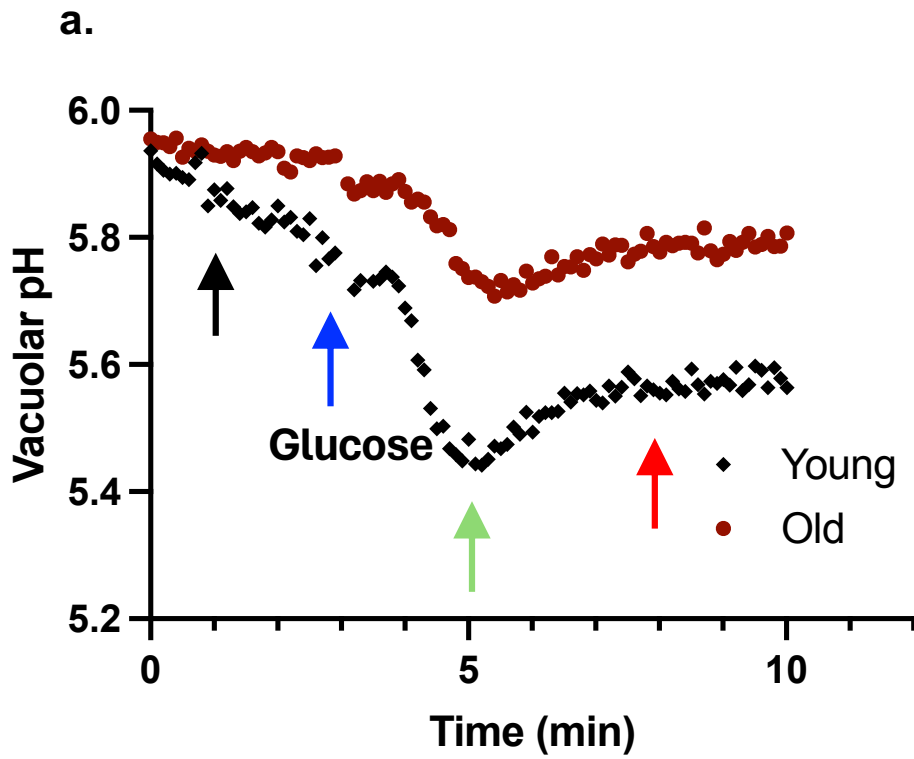
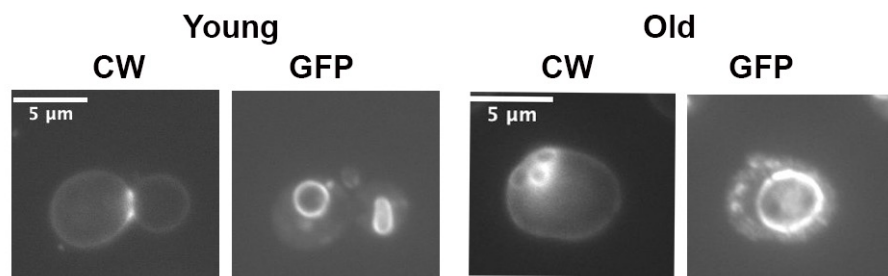
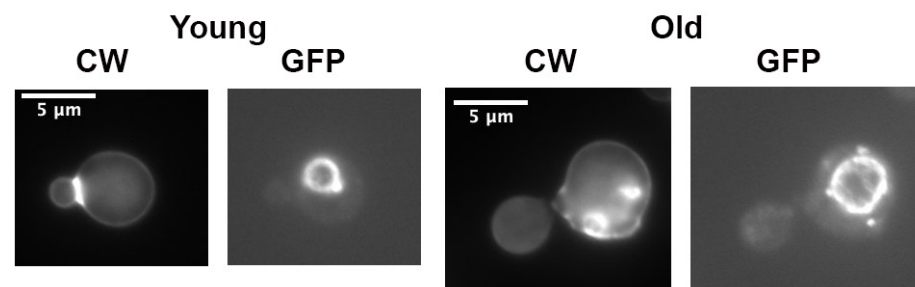


Figure 3

a. Vma5-GFP



b. Vma2-GFP



c. Vph1-GFP

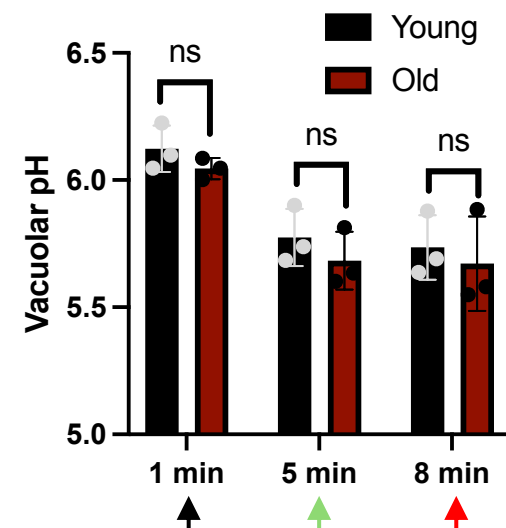
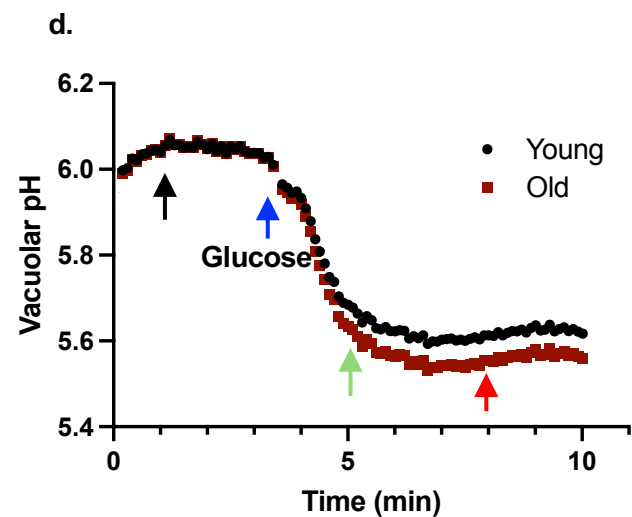
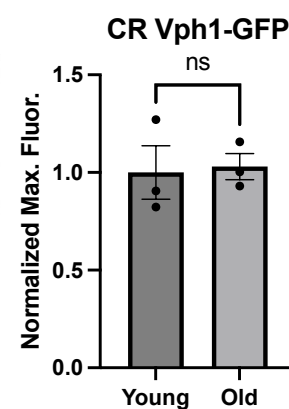
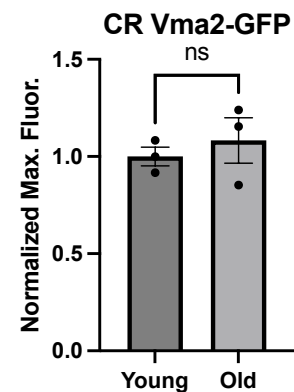
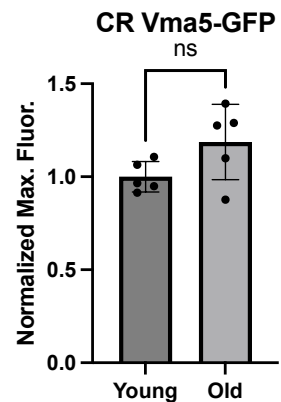
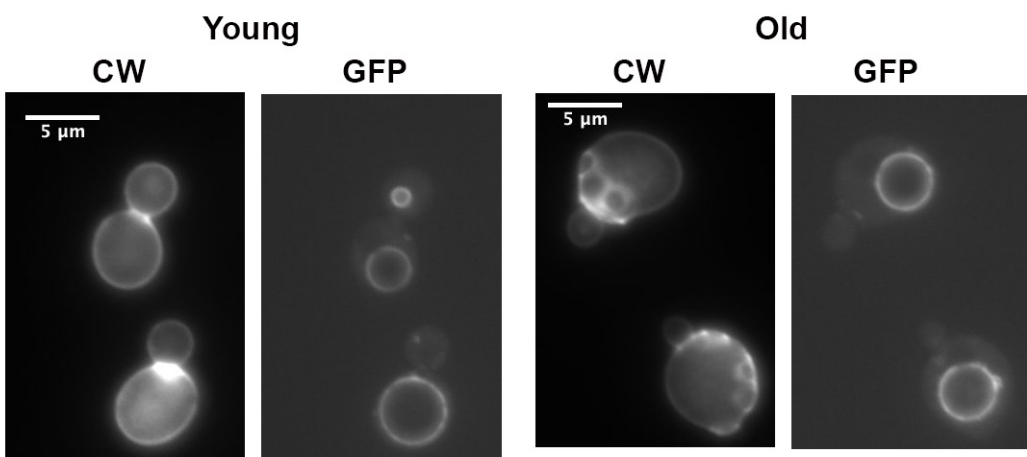


Figure 4

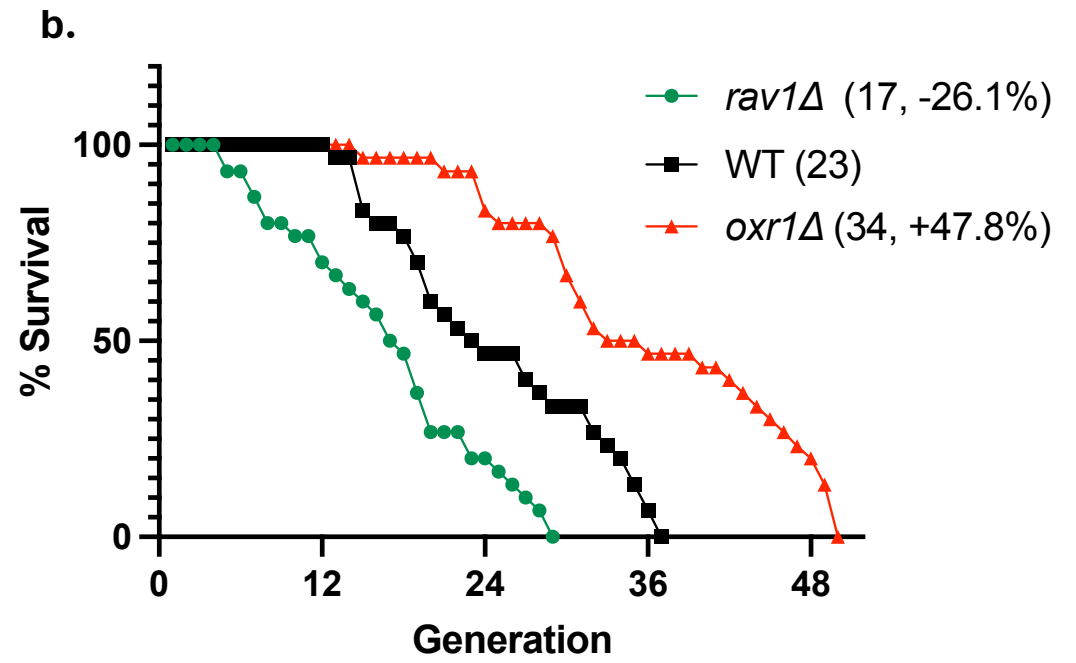
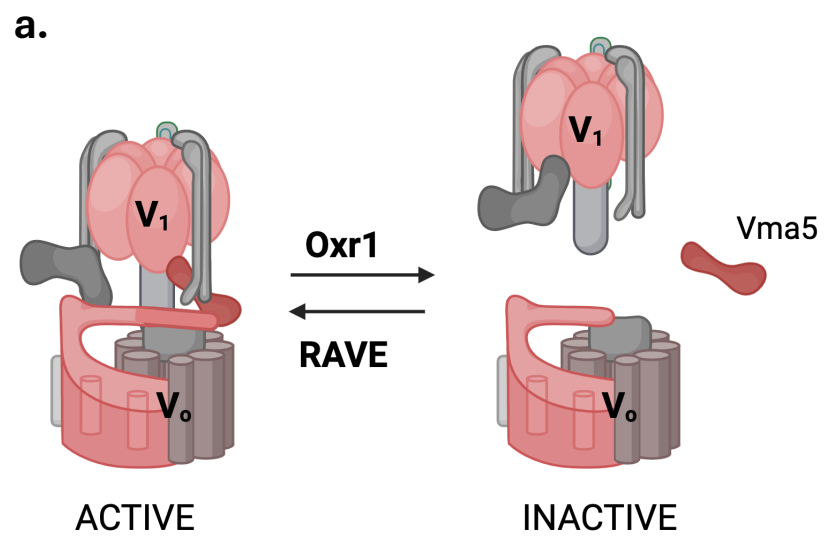


Figure 5

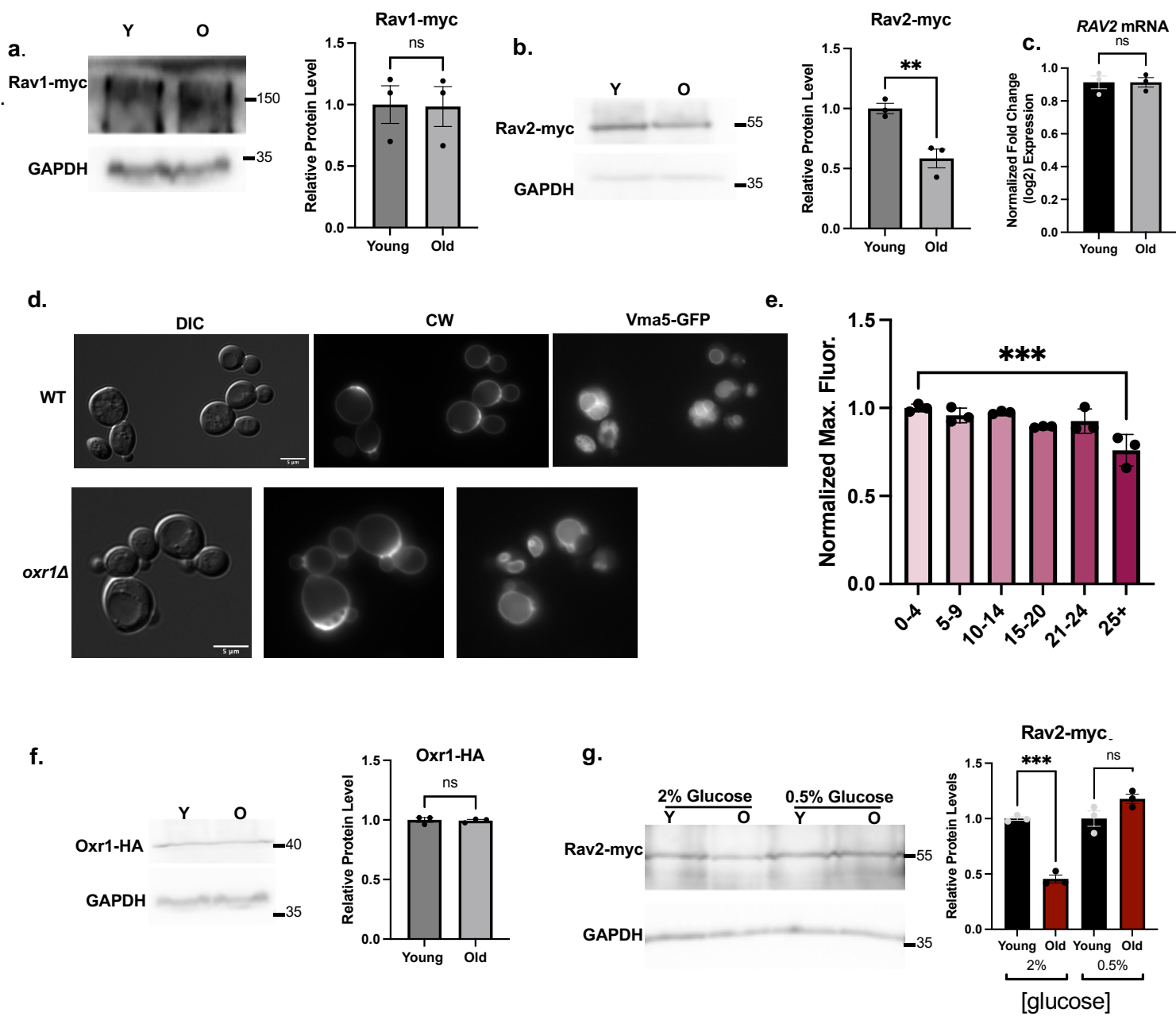


Figure 6